

Thermodynamically stable skyrmion lattice in a tetragonal frustrated antiferromagnet with dipolar interaction

Oleg I. Utesov *

B.P. Konstantinov Petersburg Nuclear Physics Institute, National Research Center “Kurchatov Institute,” Gatchina 188300, Russia;
Department of Physics, Saint Petersburg State University, St. Petersburg 198504, Russia;
and St. Petersburg School of Physics, Mathematics, and Computer Science, HSE University, 190008 St. Petersburg, Russia

 (Received 18 December 2020; revised 22 January 2021; accepted 22 January 2021; published 8 February 2021)

Motivated by recent experimental results for GdRu_2Si_2 [Khanh *et al.*, *Nat. Nanotechnol.* **15**, 444 (2020)], in which a nanometric square skyrmion lattice was observed, we propose a simple analytical mean-field description of the high-temperature part of the phase diagram of centrosymmetric tetragonal frustrated antiferromagnets with dipolar interaction in the external magnetic field. Dipolar forces provide momentum-dependent biaxial anisotropy in reciprocal space. It is shown that in a tetragonal lattice, in the large part of the Brillouin zone, for mutually perpendicular modulation vectors in the ab plane this anisotropy has mutually perpendicular easy axes and collinear middle axes, which leads to double- Q modulated spin structure stabilization. In the large part of its stability region, the latter turns out to be a square skyrmion lattice with a topological charge of ± 1 per magnetic unit cell, which is determined by the frustrated exchange coupling and thus nanometer sized. Easy and middle axes can be swapped in the presence of additional single-ion easy-axis anisotropy. This results in the different phase diagram. It is argued that the latter case is relevant to GdRu_2Si_2 .

DOI: [10.1103/PhysRevB.103.064414](https://doi.org/10.1103/PhysRevB.103.064414)

I. INTRODUCTION

Originally, skyrmions were proposed by Skyrme in 1962 to describe nucleons as topologically stable field configurations [1]. In magnetism, skyrmions emerged as metastable states in two-dimensional ferromagnets in Ref. [2]. Crucial next steps were made in seminal papers [3,4], which showed that single skyrmions and skyrmion lattices (SkLs) can be stabilized in noncentrosymmetric magnets due to the Dzyaloshinskii-Moriya interaction (DMI) [5,6]. Finally, after experimental observation of the SkL in MnSi in the so-called A phase [7], magnetic skyrmions become one of the hottest topics of contemporary physics (see, e.g., Refs. [8,9] for a review). Importantly, this interest is stimulated by promising technological applications, one of which is the racetrack memory [10].

The efficiency of possible nanodevices relies on magnetic skyrmions' nontrivial topology [2]. The topological charge of the magnetic structure is defined as the spin direction winding number on a unit sphere,

$$Q = \frac{1}{4\pi} \int \mathbf{n} \cdot [\partial_x \mathbf{n} \times \partial_y \mathbf{n}] dx dy, \quad (1)$$

where $\mathbf{n} = \mathbf{s}/|\mathbf{s}|$ is a unit vector along the averaged-over thermodynamical (and/or quantum) fluctuations' spin direction. For an individual skyrmion the integral over its size usually yields $Q = \pm 1$, whereas for the SkL the natural measure is the density of the topological charge n_{sk} . The latter quantity is of prime importance as, for instance, the topological contribution to the Hall resistivity $\rho^T \propto n_{sk}$ [11]. Note that other nontrivial

magnetic textures are actively being studied; see Ref. [12] for a review.

Recently, it became clear that skyrmions can be stabilized not only in systems with DMI. Frustrated centrosymmetric systems can also host them [13] due to anisotropic interactions. This effect was indeed observed in the frustrated triangular-lattice magnet Gd_2PdSi_3 [14]. Importantly, frustration is crucial in many multiferroics of spin origin [15], and skyrmions can lead to interesting effects in such materials [16].

Observation of the SkL in the centrosymmetric tetragonal material GdRu_2Si_2 [17] has stimulated related theoretical research [18,19]. In these papers the low-temperature part of the phase diagram was considered. It was shown that, depending on the anisotropy parameters and the external magnetic field, various phases (including topologically nontrivial ones) could emerge.

In the present study, we propose dipolar forces as the key ingredient in the stabilization of nanometer-sized skyrmions in tetragonal frustrated antiferromagnets. Previously, to the best of our knowledge, in the context of skyrmions, magnetic dipolar interaction was considered only to lead to large micrometer-sized magnetic bubbles [9,20]. Moreover, our analytical mean-field (Landau) approach is surprisingly simple in the context of topologically nontrivial spin textures.

Dipolar interaction is often small and thus negligible. However, in some materials, e.g., RbFeCl_3 [21,22], MnBr_2 [23], and MnI_2 [24], it was shown to be important anisotropic coupling. From the general arguments it should be correct for materials with magnetic ions in a spherically symmetrical state with $L = 0$ because other anisotropic interactions are moderated by the spin-orbit coupling [25]. Furthermore, dipolar forces can lead to rather complicated sequences of

*utesov@gmail.com

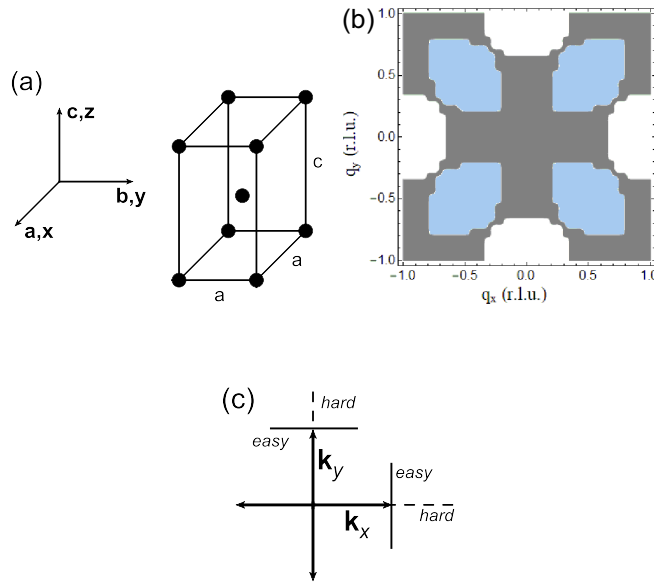


FIG. 1. (a) Tetragonal structure of $GdRu_2Si_2$ relevant to the present study; only magnetic Gd^{3+} ions are shown. (b) Using lattice parameters $a = 4.165 \text{ \AA}$ and $c = 9.61 \text{ \AA}$ of Ref. [28], one can numerically calculate the Fourier transform of the dipolar tensor [see Eq. (7)] for $|\mathbf{q}| \neq 0$. Not taking into account other possible anisotropic interactions, we found that for in-plane modulation vectors $\mathbf{q} = (q_x, q_y, 0)$ the c axis is the easy, middle, and hard one in the blue, gray, and white regions of the Brillouin zone, respectively. (c) For vectors $\pm\mathbf{k}_x = (k, 0, 0)$ and $\pm\mathbf{k}_y = (0, k, 0)$, in a wide range of k , easy axes are mutually perpendicular, and middle ones are collinear, oriented along \mathbf{c} (additional single-ion anisotropy can swap the easy and middle axes). This property of the dipolar interaction, which sometimes is referred to as the *compass anisotropy* [19,29,30], leads to the square skyrmion lattice stabilization in a certain part of the phase diagram.

phase transition at high temperatures [21,24] and at low temperatures in magnetic field [26,27]. Note that in $GdRu_2Si_2$ the magnetic Gd^{3+} ions [28] are in a state with $S = 7/2$ and $L = 0$.

Our model is based on a simple property of dipolar forces in tetragonal magnets, which provides effective momentum-dependent biaxial anisotropy. In our particular case, when the modulation vector \mathbf{q} lies in the ab plane (conventional basis vectors $\mathbf{a} \perp \mathbf{b} \perp \mathbf{c}$, $|\mathbf{a}| = |\mathbf{b}|$ are used), in the large part of the Brillouin zone the easy axis lies in plane, and the middle one is along \mathbf{c} or vice versa (see Fig. 1). This leads to the energetically effective combining of elliptical spirals with mutually perpendicular in-plane modulation vectors into the double- Q structure.

Using the mean-field approach, we show that in the case of two possible modulation vectors along the \mathbf{a} and \mathbf{b} axes (relevant to the experimental results of Ref. [17]), a peculiar sequence of phase transitions appears in the high-temperature domain of the phase diagram. First, upon temperature decreasing, the system undergoes a second-order phase transition from a paramagnetic (PM) phase to a vertical double spin-density wave state, which will be referred to as $2S$ [see Fig. 2(b)]. Next, components of the order parameters along the middle axis emerge, which manifest a continuous transi-

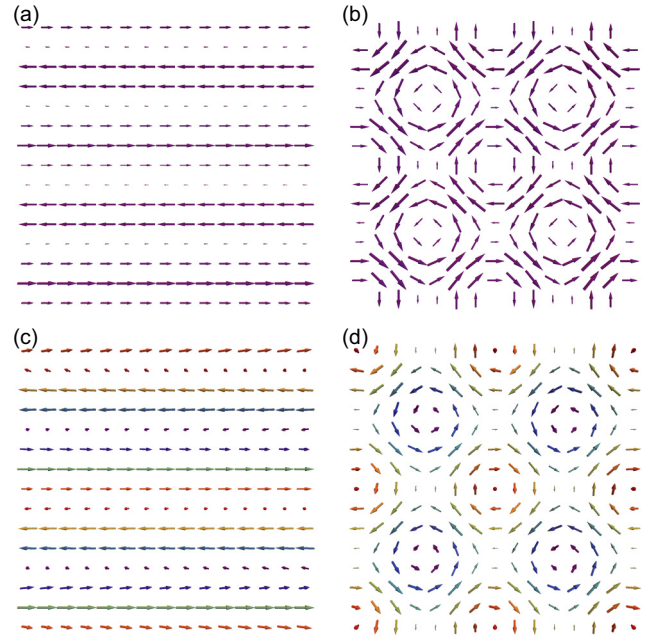


FIG. 2. Possible magnetic structures at zero external field in the ab plane; a region of 2×2 cells (with size $2\pi/k$) is shown. (a) Sinusoidal single-modulated spin-density wave ($1S$). (b) Vortical double spin-density wave ($2S$). (c) Elliptical spiral ($1Q$). (d) Double- Q elliptical phase, which consists of alternating merons and antimerons ($2Q$). In the first two structures spins lie in plane. External field uniformly magnetizes them and transforms them into simple and double-fan structures, respectively. For $1Q$ and $2Q$ spin orderings, z components of spins are shown by rainbow colors (from red, spin-up state, to magenta, spin-down state).

tion from $2S$ to the spin structure with two elliptical screw spirals combined [$2Q$; see Fig. 2(d)]. Finally, there is a first-order phase transition from the $2Q$ to single- Q elliptical spiral [$1Q$; see Fig. 2(c)]. Importantly, at nonzero magnetic fields along the c axis, the part of the phase diagram where the $2Q$ structure is the ground state becomes topologically nontrivial, being a square SkL with one (anti)skyrmion per magnetic unit cell. We also show that if the single-ion easy-axis anisotropy (which allows swapping the easy and middle axes) is taken into consideration, the phase diagram can drastically change. In this case the square SkL emerges only at magnetic fields exceeding a certain finite value, and our approach qualitatively reproduces the experimentally observed phase diagram of $GdRu_2Si_2$ [17].

The rest of the paper is organized as follows. In Sec. II we introduce the spin Hamiltonian, which consists of frustrated exchange coupling, dipolar interaction, and the Zeeman term. We also formulate the mean-field approach and discuss relevant parameters. Section III is devoted to the mean-field analysis of the high-temperature part of the temperature-magnetic field phase diagram for the case of mutually perpendicular easy axes. Free energies of the relevant spin structures are derived, and the phase boundaries are determined. In Sec. IV we discuss the topological properties of the $2Q$ phase and show that in a certain part of the phase diagram it is a square SkL. Section V addresses the case of

collinear easy axes and mutually perpendicular middle ones and the relevance to the experimental findings of Ref. [17]. Finally, Sec. VI summarizes our results and contains a related discussion.

II. MODEL

We consider a frustrated antiferromagnet on a tetragonal lattice (both simple and body centered) with one magnetic ion in a unit cell. The Hamiltonian also includes magnetodipolar interaction, single-ion anisotropy, and the Zeeman term,

$$\begin{aligned}\mathcal{H} &= \mathcal{H}_{ex} + \mathcal{H}_d + \mathcal{H}_s + \mathcal{H}_z, \\ \mathcal{H}_{ex} &= -\frac{1}{2} \sum_{i,j} J_{ij} (\mathbf{S}_i \cdot \mathbf{S}_j), \\ \mathcal{H}_d &= \frac{1}{2} \sum_{i,j} D_{ij}^{\alpha\beta} S_i^\alpha S_j^\beta, \\ \mathcal{H}_s &= -Z \sum_i (S_i^z)^2, \\ \mathcal{H}_z &= -\sum_i (\mathbf{h} \cdot \mathbf{S}_i).\end{aligned}\quad (2)$$

Here $\mathbf{h} = g\mu_B \mathbf{H}$ is the external magnetic field in energy units, and α and β denote Cartesian coordinates. For spin components we use a conventional global basis with the z coordinate along the \mathbf{c} axis and x and y along the edges of the unit cell in the ab plane (see Fig. 1). The dipolar tensor is given by

$$\mathcal{D}_{ij}^{\alpha\beta} = \omega_0 \frac{v_0}{4\pi} \left(\frac{1}{R_{ij}^3} - \frac{3R_{ij}^\alpha R_{ij}^\beta}{R_{ij}^5} \right), \quad (3)$$

where v_0 is the unit cell volume. The characteristic energy of the dipole interaction reads

$$\omega_0 = 4\pi \frac{(g\mu_B)^2}{v_0}. \quad (4)$$

This anisotropic interaction is of prime importance for magnetic ions with a half-filled electronic shell, e.g., Mn^{2+} and Eu^{2+} . For such ions $L = 0$, and dipolar forces are usually one of the most significant anisotropic terms.

After Fourier transform (N is the total number of spins)

$$\mathbf{S}_j = \frac{1}{\sqrt{N}} \sum_{\mathbf{q}} \mathbf{S}_{\mathbf{q}} e^{i\mathbf{q}\mathbf{R}_j}, \quad (5)$$

Hamiltonian (2) acquires the following form:

$$\mathcal{H}_{ex} = -\frac{1}{2} \sum_{\mathbf{q}} J_{\mathbf{q}} (\mathbf{S}_{\mathbf{q}} \cdot \mathbf{S}_{-\mathbf{q}}), \quad (6)$$

$$\mathcal{H}_d = \frac{1}{2} \sum_{\mathbf{q}} \mathcal{D}_{\mathbf{q}}^{\alpha\beta} S_{\mathbf{q}}^\alpha S_{-\mathbf{q}}^\beta. \quad (7)$$

$$\mathcal{H}_s = -Z \sum_{\mathbf{q}} S_{\mathbf{q}}^z S_{-\mathbf{q}}^z. \quad (8)$$

$$\mathcal{H}_z = -\sqrt{N} (\mathbf{h} \cdot \mathbf{S}_0). \quad (9)$$

Importantly, the first three terms here can be combined into

$$\mathcal{H}_0 = -\sum_{\mathbf{q}} \mathcal{H}_{\mathbf{q}}^{\alpha\beta} S_{\mathbf{q}}^\alpha S_{-\mathbf{q}}^\beta, \quad (10)$$

where 0 denotes the Hamiltonian at $h = 0$. Tensor $\mathcal{H}_{\mathbf{q}}^{\alpha\beta}$ has three eigenvalues $\lambda_1(\mathbf{q}) \geq \lambda_2(\mathbf{q}) \geq \lambda_3(\mathbf{q})$ corresponding to three eigenvectors $\mathbf{v}_1(\mathbf{q})$, $\mathbf{v}_2(\mathbf{q})$, $\mathbf{v}_3(\mathbf{q})$ at each momentum. The latter define the particular basis of the easy, middle, and hard axes for each \mathbf{q} . This momentum-dependent biaxial anisotropy is due to dipolar forces.

The dipolar tensor in reciprocal space $\mathcal{D}_{\mathbf{q}}^{\alpha\beta}$ can be calculated numerically using a standard technique involving rewriting it in a fast convergent form (see Ref. [31] and references therein). Moreover, at high temperatures (close to the transition to the paramagnetic phase) only particular \mathbf{q} are important, which significantly simplifies the corresponding analysis [24]. Since dipolar forces are usually small in comparison with exchange coupling, these momenta are close to those where $J_{\mathbf{q}}$ has (local) maxima. The latter are assumed to be incommensurate due to the frustration. Thus, at low temperatures and small h , some sort of a spiral ordering is the ground state of the system.

Below we shall mostly discuss the particular case where magnetic ordering modulation vectors are oriented along the \mathbf{a} and \mathbf{b} axes, with $\mathbf{k}_x = (k, 0, 0)$ and $\mathbf{k}_y = (0, k, 0)$. Not taking into account the possible effect of the single-ion anisotropy, we arrive at a crucial point for the present theory: over a wide range of parameters of the tetragonal lattice, it can be shown numerically that the easy axis for \mathbf{k}_x is \mathbf{b} , the hard one is \mathbf{a} , and the reverse is true for \mathbf{k}_y . The middle axis is \mathbf{c} for the both vectors (see Fig. 1). This is exactly realized in the case of GdRu_2Si_2 , where $k = 0.22$ in reciprocal lattice units [17] (in the notation used below $k = 0.22 \times 2\pi/a$). Furthermore, this provides a simple physical ground for anisotropic momentum-dependent terms used in recent theoretical studies [18,19] (compass anisotropy), which was previously attributed to the spin-orbit coupling [29].

We point out that the frustration can lead to competition with incommensurate structures characterized by another momentum with a close value of $J_{\mathbf{q}}$. In the general case, the corresponding local axis basis will not possess the feature described above. For instance, if the modulation vector $\mathbf{q} \parallel \mathbf{c}$, the dipolar tensor simply makes the ab plane an easy one. It can further complicate the phase diagram, introducing some additional intermediate phases.

In our high-temperature calculations we shall use s_i for the mean value of the corresponding spin operator \mathbf{S}_i . It can be shown that the mean-field free energy can be expressed as (see, e.g., Refs. [24,32] for details)

$$\mathcal{F} = -\sum_{\mathbf{q}} \mathcal{H}_{\mathbf{q}}^{\alpha\beta} s_{\mathbf{q}}^\alpha s_{-\mathbf{q}}^\beta - \sqrt{N} \mathbf{h} \cdot \mathbf{s}_0 + AT \sum_i s_i^2 + BT_c \sum_i s_i^4, \quad (11)$$

provided that $|s_i| \ll S$; $T_c = \lambda_1(\mathbf{k}_x)/A$ is the temperature of the phase transition from the paramagnetic to magnetically ordered state at $h = 0$. The particular phase will be specified below. Expansion parameters A and B are given by

$$A = \frac{3}{2S(S+1)}, \quad (12)$$

$$B = \frac{9[(2S+1)^4 - 1]}{20(2S)^4(S+1)^4}. \quad (13)$$

For $S = 7/2$ one has $A \approx 0.095$ and $B \approx 0.002$.

In order to make a connection with real materials, we estimate the relevant parameters using the experimental data of Ref. [17]. For the case without single-ion anisotropy ($Z = 0$) using only the ordering temperature $T_c(B = 0) \approx 45$ K, the saturation field $B_{\text{sat}}(T = 0) \approx 10$ T [33], and the numerically calculated dipolar tensor, we get (all values are in kelvins)

$$\begin{aligned} \lambda_1 &\approx 4.3, & J_0 &\approx 4.6, \\ \lambda_1 - \lambda_2 &\approx 0.05, & \lambda_1 - \lambda_3 &\approx 0.20, \end{aligned} \quad (14)$$

where λ_i are the same for \mathbf{k}_x and \mathbf{k}_y .

III. MEAN-FIELD APPROACH FOR IN-PLANE EASY AXES

In this section, we perform mean-field analysis based on the smallness of the order parameters at high temperatures. For definiteness, we consider the particular case of possible modulation vectors, and the corresponding axis sets depicted in Fig. 1(c).

A. Spin structures at $h = 0$

We start with the simplest case without the external field. In systems with tetragonal symmetry due to four energy minima of the exchange interaction (at momenta $\pm\mathbf{k}_x$ and $\pm\mathbf{k}_y$), along with a conventional single-modulated sinusoidal spin-density wave (SDW) and elliptical (helical) phases, the so-called double structures can emerge. Below we calculate the free energy of each of the relevant spin structures, shown in Fig. 2. Note that due to the symmetry of the system and, consequently, J_q , the formation of triple structures, e.g., a triangular SkL, in general is energetically disadvantageous and is not considered below.

1. Single- Q spin-density wave (1S)

In this case (taking, for definiteness, \mathbf{k}_x as the modulation vector; \mathbf{k}_y evidently yields the same result)

$$\mathbf{s}_i = s\mathbf{e}_y \cos \mathbf{k}_x \mathbf{R}_i. \quad (15)$$

Using Eq. (11), we get

$$\frac{\mathcal{F}}{N} = -\frac{s^2\lambda_1}{2} + \frac{s^2AT}{2} + \frac{3s^4BT_c}{8}. \quad (16)$$

Minimization with respect to s gives (for $T \leq T_c$)

$$s^2 = \frac{2(\lambda_1 - AT)}{3BT_c} \quad (17)$$

and

$$\frac{\mathcal{F}_{1S}}{N} = -\frac{(\lambda_1 - AT)^2}{6BT_c}. \quad (18)$$

2. Double- Q spin-density wave (2S)

According to the symmetry of the system, the double- Q spin-density wave with both order parameters along the local easy axis becomes possible. The corresponding spin ordering reads

$$\mathbf{s}_i = s(\mathbf{e}_y \cos \mathbf{k}_x \mathbf{R}_i + \mathbf{e}_x \cos \mathbf{k}_y \mathbf{R}_i). \quad (19)$$

In real space this is the vortex structure depicted in Fig. 2(b). Note that due to the system translational invariance and

incommensurability of the modulation vectors, the phases of trigonometric functions are not important here and can be taken to be arbitrary. Using Eq. (11), one gets

$$\frac{\mathcal{F}}{N} = -s^2\lambda_1 + s^2AT + \frac{5s^4BT_c}{4}. \quad (20)$$

Minimization with respect to s yields

$$s^2 = \frac{2(\lambda_1 - AT)}{5BT_c} \quad (21)$$

and

$$\frac{\mathcal{F}_{2S}}{N} = -\frac{(\lambda_1 - AT)^2}{5BT_c}. \quad (22)$$

The last quantity is always smaller than the free energy of the single- Q SDW (18). As a corollary, at T_c the system undergoes a phase transition between the paramagnetic (PM) phase and the double- Q vortex structure. The complementary low-temperature result at high magnetic field along the \mathbf{c} axis is the appearance of a double- Q phase magnetized along the field and vortical in the perpendicular plane instead of single- Q fan one [18].

3. Single- Q elliptical phase (1Q)

We further proceed with an elliptical structure modulated along one direction (\mathbf{k}_x is taken for definiteness):

$$\mathbf{s}_i = s_1\mathbf{e}_y \cos \mathbf{k}_x \mathbf{R}_i + s_2\mathbf{e}_z \sin \mathbf{k}_x \mathbf{R}_i. \quad (23)$$

The chirality of this structure is not important; one can freely vary the sign of the second term and the common phase for sine and cosine functions.

The corresponding free energy reads

$$\begin{aligned} \frac{\mathcal{F}}{N} = & -\frac{s_1^2\lambda_1 + s_2^2\lambda_2}{2} + \frac{(s_1^2 + s_2^2)AT}{2} \\ & + \frac{(3s_1^4 + 2s_1^2s_2^2 + 3s_2^4)BT_c}{8}. \end{aligned} \quad (24)$$

Nonzero s_2 emerges at $T < T_{1Q} = T_c - 3(\lambda_1 - \lambda_2)/2A$; the spin components are given by

$$\begin{aligned} s_1^2 &= \frac{2(\lambda_1 - AT) + (\lambda_1 - \lambda_2)}{4BT_c}, \\ s_2^2 &= \frac{2(\lambda_1 - AT) - 3(\lambda_1 - \lambda_2)}{4BT_c}. \end{aligned} \quad (25)$$

So the free energy has the following form:

$$\begin{aligned} \frac{\mathcal{F}_{1Q}}{N} &= -\frac{4(\lambda_1 - AT)^2 - 4(\lambda_1 - AT)(\lambda_1 - \lambda_2) + 3(\lambda_1 - \lambda_2)^2}{16BT_c}. \end{aligned} \quad (26)$$

Below we consider magnetic field along the \mathbf{c} axis, so similar to the 1Q phase, a conical phase with spins rotating in the ab plane (we shall refer to it as XY) can emerge. At zero field its free energy is given by Eq. (26) with the substitution $\lambda_2 \rightarrow \lambda_3$.

4. Double- Q elliptical phase ($2Q$)

We turn to a superposition of two single- Q elliptical structures with mutually perpendicular modulation vectors \mathbf{k}_x and \mathbf{k}_y . This structure will be referred to as $2Q$. The corresponding spin arrangement is given by

$$\begin{aligned} \mathbf{s}_i = & s_1(\mathbf{e}_y \cos \mathbf{k}_x \mathbf{R}_i + \mathbf{e}_x \cos \mathbf{k}_y \mathbf{R}_i) \\ & + s_2 \mathbf{e}_z (\sin \mathbf{k}_x \mathbf{R}_i + \sin \mathbf{k}_y \mathbf{R}_i). \end{aligned} \quad (27)$$

As before, the chiralities and phases of both components can be arbitrary: they do not affect the free energy.

The corresponding free energy reads

$$\begin{aligned} \frac{\mathcal{F}}{N} = & -(s_1^2 \lambda_1 + s_2^2 \lambda_2) + (s_1^2 + s_2^2) AT \\ & + \frac{(5s_1^4 + 6s_1^2 s_2^2 + 9s_2^4) BT_c}{4}. \end{aligned} \quad (28)$$

This structure is possible if $T < T_{2Q} = T_c - 5(\lambda_1 - \lambda_2)/2A$. The order parameters are as follows:

$$\begin{aligned} s_1^2 = & \frac{2(\lambda_1 - AT) + (\lambda_1 - \lambda_2)}{6BT_c}, \\ s_2^2 = & \frac{2(\lambda_1 - AT) - 5(\lambda_1 - \lambda_2)}{18BT_c}, \end{aligned} \quad (29)$$

and the free energy has the form

$$\begin{aligned} \frac{\mathcal{F}_{2Q}}{N} \\ = & -\frac{8(\lambda_1 - AT)^2 - 4(\lambda_1 - AT)(\lambda_1 - \lambda_2) + 5(\lambda_1 - \lambda_2)^2}{36BT_c}. \end{aligned} \quad (30)$$

To conclude this section, we point out that it can be shown that the double-XY structure has larger free energy than the simple one and should not be considered.

B. Sequence of phase transitions at $h = 0$

The analytical equations presented above for the free energy of different phases implicitly depend on the corresponding modulation vectors through λ_i 's ($i = 1, 2$) \mathbf{q} dependence. For the $2S$ vortical structure [see Eq. (22)] it is evident that the modulation vector corresponds to the maximal value of $\lambda_1(\mathbf{q})$ (such a \mathbf{q} is referred to as \mathbf{k}_x or \mathbf{k}_y). However, for other phases it is not completely true due to the possibility of different behaviors of $\lambda_1(\mathbf{q})$ and $\lambda_2(\mathbf{q})$ at these points. It can shift the structure modulation vector (which was, indeed, observed in Ref. [17]). Nevertheless, since isotropic exchange interaction is typically much larger than the dipolar forces, we neglect this small effect below and do not write the \mathbf{q} dependence of λ_i .

For the phase transition treatment, we first simplify the notation: let $t = \lambda_1 - AT$ (in the magnetically ordered phases $t > 0$) and $\Lambda = \lambda_1 - \lambda_2 > 0$. Then, one should compare the following "free energies":

$$\begin{aligned} f_{2S} = & -\frac{t^2}{5}, \quad \frac{5\Lambda}{2} \geq t > 0, \\ f_{1Q} = & -\frac{4t^2 - 4\Lambda t + 3\Lambda^2}{16}, \quad t > \frac{3\Lambda}{2}, \\ f_{2Q} = & -\frac{8t^2 - 4\Lambda t + 5\Lambda^2}{36}, \quad t > \frac{5\Lambda}{2}. \end{aligned} \quad (31)$$

The smallest one at a given t indicates the ground state of the system.

Naturally, at $t \gg \Lambda$ the $1Q$ phase (single- Q elliptical spiral) is the ground state. A possible first-order phase transition between $2S$ and $1Q$ can be determined from the equation

$$\frac{t^2}{5} = \frac{4t^2 - 4\Lambda t + 3\Lambda^2}{16}. \quad (32)$$

Corresponding solutions read

$$t = \frac{5 \pm \sqrt{10}}{2} \Lambda \approx 0.9\Lambda, 4.1\Lambda. \quad (33)$$

Evidently, they are nonphysical: the one with the plus sign is larger than $t_{2Q} = 2.5\Lambda$, at which the $2Q$ structure emerges and substitutes for $2S$. The other one with a minus is smaller than $t_{1Q} = 1.5\Lambda$, which is the boundary for $1Q$ (meta)stability. Thus, if one neglects the possibility of different values of k for $1Q$ and $2Q$, the following scenario of phase transitions upon temperature variation takes place: $PM \leftrightarrow 2S \leftrightarrow 2Q \leftrightarrow 1Q$. The first two are second-order phase transitions. The third one is of the first order; the corresponding "temperature" is given by

$$t_S = \frac{5 + 3\sqrt{2}}{2} \Lambda \approx 4.6\Lambda. \quad (34)$$

C. Nonzero magnetic field and phase diagram

For definiteness we consider magnetic field only along the tetragonal \mathbf{c} axis. It results in a finite homogeneous spin component along it. We assume that the system is far from the ferromagnetic transition critical point near T_c , $\Lambda \ll AT_c - \lambda_0$. Here for the ellipsoidal shape of the sample $\lambda_0 = (\mathbf{J}_0 - \omega_0 \mathcal{N}_{zz})/2$, with \mathcal{N}_{zz} being the corresponding demagnetization tensor component [34]. So the spin ordering of each phase acquires the correction $\delta \mathbf{s}_i = m \mathbf{e}_z$, which can be determined using the Curie-Weiss law:

$$m = \chi(T)h = \frac{h}{2(AT - \lambda_0)}, \quad (35)$$

provided that the high-temperature mean-field expansion (11) is correct (T close to T_c). Note that $\chi(t)$ is almost constant in this region and can be substituted by $\chi \equiv \chi(T_c)$.

We further proceed with the influence of magnetic field on different spin structures. All the relevant spin orderings (19), (23), and (27) now have the additional term $m \mathbf{e}_z$. For the free energies of various phases presented above it means the appearance of new (proportional to the squared order parameters and squared magnetization) terms originating from the $BT_c \sum_i s_i^4$ part of the free energy (11). In the expressions for the order parameters derived above and related free energies the following renormalizations should be done: (i) one should make the effective "temperature" change $t \rightarrow t' = t - 2BT_c(\chi h)^2$ for $2S$, and (ii) for $1Q$ and $2Q$ along with $t \rightarrow t'$ one should also substitute Λ with $\Lambda' = \Lambda + 4BT_c(\chi h)^2$. Importantly, t' and Λ' should be directly plugged into free energies (31). The additional contribution from the magnetic field is identical for all the phases, being equal to $-\chi h^2/2$, so it can be omitted.

However, one should bear in mind that for conical XY ordering at $h = 0$ there is no z component of the order param-

eter, and its interaction with magnetic field leads to a different with $1Q$ effect. The XY structure is similar to that of $1Q$, but modulated spin components are in the ab plane:

$$\mathbf{s}_i = s_1 \mathbf{e}_y \cos \mathbf{k}_x \mathbf{R}_i + s_2 \mathbf{e}_x \sin \mathbf{k}_x \mathbf{R}_i + m \mathbf{e}_z. \quad (36)$$

Note that the spin component $\propto s_2$ is along the hard axis. Let $\Lambda'' = \lambda_1 - \lambda_3 > \Lambda$. So the XY free energy at $h = 0$ reads

$$f_{XY} = -\frac{4t^2 - 4\Lambda''t + 3\Lambda''^2}{16}, \quad t > \frac{3\Lambda''}{2}. \quad (37)$$

In magnetic field one should change the “temperature” $t \rightarrow t'$ like for the other phases. However, Λ'' stays intact. This, along with other effects, leads to the spiral plane flop (transition $1Q \leftrightarrow XY$, which is well known for frustrated antiferromagnets with dipolar interaction; see Ref. [35]) at certain h_{SF} for which $\Lambda' = \Lambda''$. One obtains

$$h_{SF} = \sqrt{\frac{\Lambda'' - \Lambda}{4BT_c\chi^2}}, \quad (38)$$

which is almost constant upon temperature variation.

Using the simple relations presented above, we can derive analytical expressions for the phase boundaries. First, the boundary between PM (or the field-induced ferromagneticlike collinear state) and $2S$ is given by

$$t_c(h) = 2BT_c\chi^2h^2. \quad (39)$$

Next, the second-order phase transition curve between $2S$ and $2Q$ is as follows:

$$t_{2Q}(h) = \frac{5\Lambda}{2} + 12BT_c\chi^2h^2. \quad (40)$$

At $h < h_{SF}$ there is also a boundary between the $1Q$ and $2Q$ phases,

$$t_S(h) = 4.6\Lambda + 20.4BT_c\chi^2h^2. \quad (41)$$

Phase boundaries which include XY [see also Eq. (38)] are as follows. (i) With the $2S$ phase the phase boundary reads

$$t_{XY-2S}(h) = 4.1\Lambda'' + 2BT_c\chi^2h^2. \quad (42)$$

(ii) With the $2Q$ phase the expression is rather cumbersome:

$$t_{XY-2Q}(h) = 2BT_c\chi^2h^2 + \frac{9\Lambda'' - 4\Lambda' + 3\sqrt{4(\Lambda'' - \Lambda')^2 + 2\Lambda''^2}}{2}. \quad (43)$$

We would like to point out that exact numerical minimization of the free energy (11) in the magnetic field does not change the phase boundaries presented above significantly.

Before considering the phase diagram for a particular parameter set, let us have a closer look at Eq. (43) at $h = h_{SF}$. In fact, it is determining the position of the triple point where $1Q$, $2Q$, and XY are in equilibrium. Using Eqs. (43) and (38), we get

$$t_{tr} \approx (\Lambda'' - \Lambda)/2 + 4.6\Lambda''. \quad (44)$$

The difference between λ_i values is usually of the order of 0.1 K [see Eq. (14)], which provides the estimation $t_{tr} \sim 1$ K, and (using $A \sim 0.1$) $T_c - T_{tr} \sim 10$ K in standard units. In

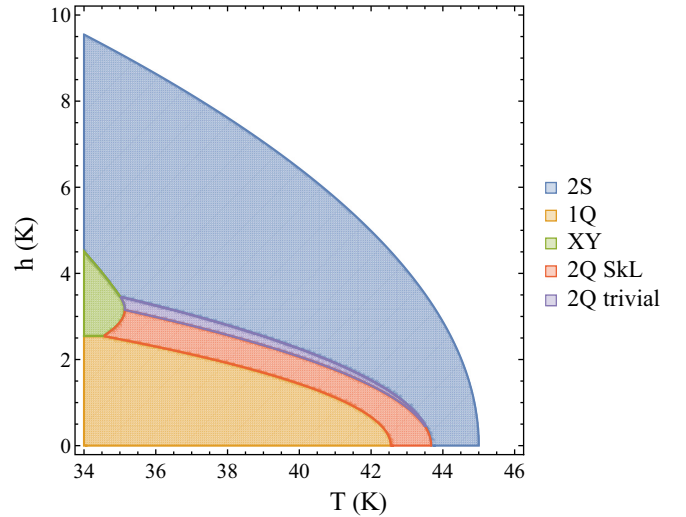


FIG. 3. High-temperature part of the phase diagram for a centrosymmetric tetragonal frustrated antiferromagnet with two possible mutually perpendicular modulation vectors and dipolar interaction (see Fig. 1). The parameters in (14) were used. Depending on magnetic field and temperature, the $2Q$ phase can be either topologically trivial or not (see text). The conical XY phase emerges beyond the theory applicability region and is shown only for illustration purposes.

real systems in that region of the phase diagram $|s_i| \sim S$, and Landau expansion breaks down, thus making predictions involving the conical XY phase unreliable.

Let us proceed with the particular example of the phase diagram for the set of parameters (14). In this case $\lambda_0 \approx 2.3$ K, which justifies the approximation of constant susceptibility in the relevant part of the phase diagram, which we draw in Fig. 3. Near the triple point ($t_{tr} \approx 1.06$ K), where XY can come into play, using Eqs. (25), one has $s_1 \approx 2.5$ and $s_2 \approx 2.4$, which means that our approach essentially fails at such temperatures. This raises an important question, whether the XY conical phase, which, as seen in Fig. 3, can terminate the $2Q$ phase region, emerges at low temperatures in reality or not.

IV. TOPOLOGICAL PROPERTIES OF THE $2Q$ PHASE

Using Eq. (1), it is easy to show that $2S$, $1Q$, and XY are, as always, topologically trivial; $n_{sk} = 0$.

Let us turn to the $2Q$ structure. First of all, using Eq. (27), we rewrite the spin ordering in magnetic field in the following form:

$$\mathbf{s}(x, y) = \begin{pmatrix} s_1 \sin ky \\ -s_1 \sin kx \\ s_2 [\cos kx + \cos ky] + m \end{pmatrix}. \quad (45)$$

The magnetic unit cell is a square with the size $(2\pi/k) \times (2\pi/k)$. Note that for illustration purposes we take the particular structure with $s_1, s_2, m > 0$. Its counterparts with other relative phases and chiralities for two elliptical components can be analyzed in a similar way. These variations can be accompanied by a change in signs of the corresponding

topological charges (e.g., skyrmions can be substituted by antiskyrmions).

At zero field magnetic ordering has an important antisymmetry property: $\mathbf{s}(x, y) = -\mathbf{s}(x \pm \pi/k, y \pm \pi/k)$. This is equivalent to $\langle n_{sk} \rangle = 0$ ($\langle \dots \rangle$ is averaged over the magnetic unit cell quantity). However, the magnetic ordering is somewhat nontrivial, and the structure consists of core-down merons with $Q = -1/2$ and core-up antimerons with $Q = +1/2$ (see Fig. 1 of Ref. [36] for the details) alternating in a square lattice, as shown in Fig. 2(d).

Nonzero h breaks the above-mentioned antisymmetry, and the magnetic ordering becomes topologically nontrivial with $Q = -1$ per magnetic unit cell. At small h , which results in $m \ll s_1, s_2$, the latter can be understood as follows. One can neglect m in the spin ordering (45) almost everywhere except for a small neighborhood (its radius is $\sim \sqrt{m/s_2} \ll 1$) of points with coordinates $(\pi/k, 0)$, $(0, \pi/k)$, and equivalent to them. In these regions core-up merons with $Q = -1/2$ emerge at $h > 0$ [see Fig. 4(a)]. One has four halves of such merons in the magnetic unit cell; thus, $n_{sk} = -1$. At moderate h , for which $m \sim s_1, s_2$, the boundary between core-up merons and core-up antimerons is no longer pronounced, and the whole magnetic structure can be considered a square skyrmion lattice [see Fig. 4(b)]. Under a further magnetic field increase (when the condition $m < 2s_2$ is violated) the magnetic structure becomes topologically trivial since all spin z components are positive.

We proceed with the phase diagram established in the previous section. Evidently, the whole region of the $2Q$ phase stability cannot be topologically nontrivial because $s_2 \ll 1$ near its boundary with $2S$. At given h , in order to have a skyrmion lattice, the condition $4s_2^2 > m^2 = \chi^2 h^2$ should be fulfilled, where

$$s_2^2 = \frac{2t' - 5\Lambda'}{18BT_c}. \quad (46)$$

Using these formulas, one can define the boundary for the SkL region inside the $2Q$ one as [see Eq. (40)]

$$t_{SkL}(h) = t_{2Q}(h) + \delta t(h), \quad \delta t(h) = \frac{9}{4}BT_c\chi^2 h^2. \quad (47)$$

Importantly, it is smaller than $t_S(h)$ [see Eq. (41)]. Figure 3 illustrates these statements.

V. MEAN-FIELD APPROACH FOR COLLINEAR OUT-OF-PLANE EASY AXES

The consideration above relies on small single-ion anisotropy, which cannot alter the axis hierarchy established by dipolar interaction [see Fig. 1(c)]. However, this case yields a substantially different phase diagram (see Fig. 3), in comparison with the experimentally observed one in Ref. [17]. Here we consider significant single-ion anisotropy, which makes the \mathbf{c} axis the easy one for both modulation vectors \mathbf{k}_x and \mathbf{k}_y . Mathematically, in comparison with the pure dipolar case ($Z = 0$) the eigenvalues change as follows: $\lambda_1 \rightarrow \lambda_1 - Z$, $\lambda_2 \rightarrow \lambda_2 + Z$, $\lambda_3 \rightarrow \lambda_3 - Z$. So for $Z > (\lambda_1 - \lambda_2)/2$ the hard axes stay intact; however, the easy and middle ones are swapped.

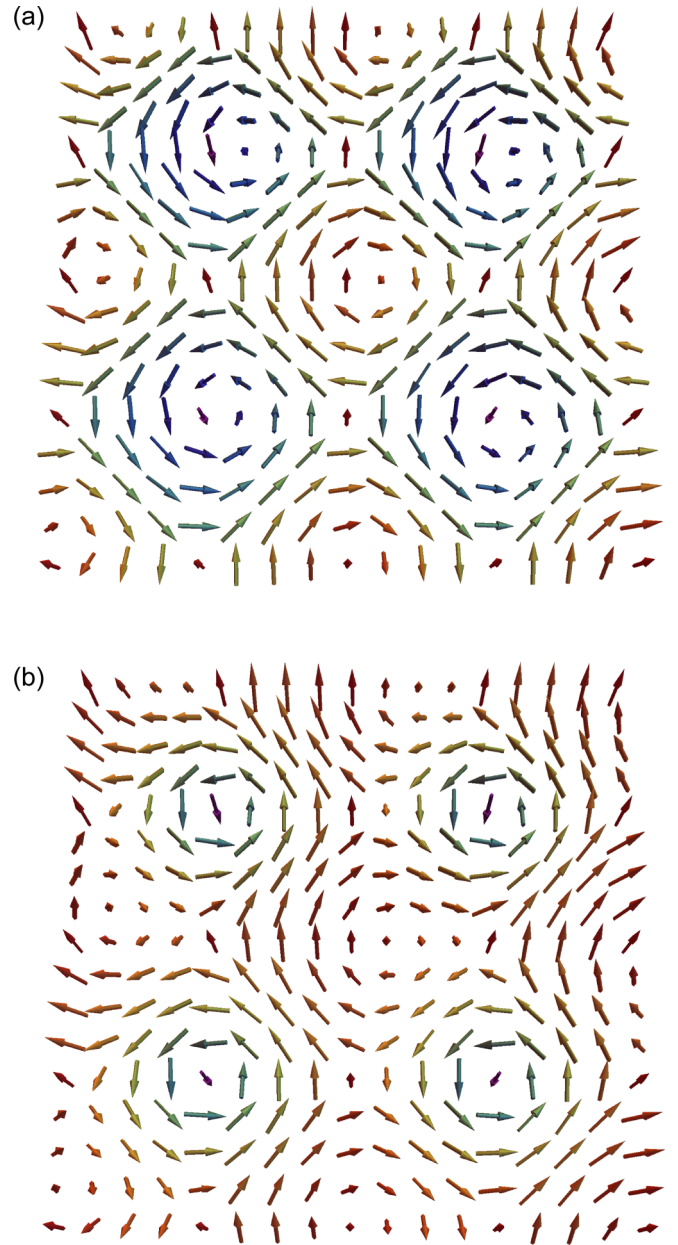


FIG. 4. Sketch of the $2Q$ spin ordering in applied magnetic field; part of the ab plane with a size of 2×2 magnetic unit cells is shown. (a) At small magnetic fields in comparison with the zero-field case [see Fig. 2(d)], additional small core-up merons emerge, providing topological charge $Q = -1$ per unit cell. (b) At larger fields, the boundary between core-up merons and antimerons vanishes, and the magnetic ordering represents a square skyrmion lattice.

We continue to use $\lambda_1 \geq \lambda_2 \geq \lambda_3$ in the mean-field analysis below, bearing in mind that the easy direction is now along the \mathbf{c} axis.

A. Spin structures

Here we briefly discuss relevant spin structures at both $h = 0$ and $h \neq 0$.

1. Single- Q spin-density wave (1S)

The spin ordering of 1S reads

$$\mathbf{s}_i = s \mathbf{e}_z \cos \mathbf{k}_x \mathbf{R}_i, \quad (48)$$

where

$$s^2 = \frac{2(\lambda_1 - AT)}{3BT_c} = \frac{2t}{3BT_c}. \quad (49)$$

The corresponding free energy is given by (see Sec. III B)

$$f_{1S} = -\frac{t^2}{6}, \quad 3\Lambda/2 \geq t > 0. \quad (50)$$

At larger $t > 3\Lambda/2$, it transforms into the $1Q$ structure (see below).

In the external magnetic field one should make the substitution $t \rightarrow t' = t - 6BT_c(\chi h)^2$.

2. Double- Q spin-density wave (2S)

In comparison with Sec. III, here the vortical structure involves two middle axes. This immediately affects the phase diagram, as shown below. The $2S$ spin structure reads

$$\mathbf{s}_i = s(\mathbf{e}_x \cos \mathbf{k}_y \mathbf{R}_i + \mathbf{e}_y \cos \mathbf{k}_x \mathbf{R}_i), \quad (51)$$

where

$$s^2 = \frac{2(\lambda_2 - AT)}{5BT_c} = \frac{2(t - \Lambda)}{5BT_c}. \quad (52)$$

The free energy is given by

$$f_{2S} = -\frac{(t - \Lambda)^2}{5}, \quad t > \Lambda. \quad (53)$$

So in the considered case there is always a range of parameters for which $1S$ is preferable in comparison with $2S$, which should be contrasted with the results of Sec. III.

In the magnetic field, one should make the change $t \rightarrow t' = t - 2BT_c(\chi h)^2$.

3. Single- Q elliptical phase (1Q)

In this case spin ordering reads

$$\mathbf{s}_i = s_1 \mathbf{e}_z \cos \mathbf{k}_x \mathbf{R}_i + s_2 \mathbf{e}_y \cos \mathbf{k}_x \mathbf{R}_i, \quad (54)$$

where

$$s_1^2 = \frac{2(\lambda_1 - AT) + (\lambda_1 - \lambda_2)}{4BT_c} = \frac{2t + \Lambda}{4BT_c}, \quad (55)$$

$$s_2^2 = \frac{2(\lambda_1 - AT) - 3(\lambda_1 - \lambda_2)}{4BT_c} = \frac{2t - 3\Lambda}{4BT_c}.$$

The corresponding free energy is as follows:

$$f_{1Q} = -\frac{4t^2 - 4\Lambda t + 3\Lambda^2}{16}, \quad t > 3\Lambda/2 \wedge t > -\Lambda/2. \quad (56)$$

The last inequality becomes important in magnetic field, where one should use $t' = t - 6BT_c(\chi h)^2$ and $\Lambda' = \Lambda - 4BT_c(\chi h)^2$.

For the XY phase with spins rotating in the ab plane, one has

$$f_{XY} = -\frac{4(t - \Lambda)^2 - 4(t - \Lambda)(\Lambda'' - \Lambda) + 3(\Lambda'' - \Lambda)^2}{16},$$

$$t > \frac{3\Lambda'' - \Lambda}{2}. \quad (57)$$

The substitution $t \rightarrow t' = t - 2BT_c(\chi h)^2$ should be done in the external field, whereas Λ'' and Λ stay intact.

4. Double- Q elliptical phase (2Q)

Spin ordering in the double- Q phase is given by

$$\begin{aligned} \mathbf{s}_i = & s_1 \mathbf{e}_z (\cos \mathbf{k}_x \mathbf{R}_i + \cos \mathbf{k}_y \mathbf{R}_i) \\ & + s_2 (\mathbf{e}_y \sin \mathbf{k}_x \mathbf{R}_i + \mathbf{e}_x \sin \mathbf{k}_y \mathbf{R}_i). \end{aligned} \quad (58)$$

The order parameters are as follows:

$$\begin{aligned} s_1^2 &= \frac{2(\lambda_2 - AT) - 5(\lambda_2 - \lambda_1)}{18BT_c} = \frac{2t + 3\Lambda}{18BT_c}, \\ s_2^2 &= \frac{2(\lambda_2 - AT) + (\lambda_2 - \lambda_1)}{6BT_c} = \frac{2t - 3\Lambda}{6BT_c}. \end{aligned} \quad (59)$$

The free energy has the form

$$f_{2Q} = -\frac{8t^2 - 12\Lambda t + 9\Lambda^2}{36}, \quad t > 3\Lambda/2 \wedge t > -3\Lambda/2. \quad (60)$$

As for the $1Q$ phase, one should use $t' = t - 6BT_c(\chi h)^2$ and $\Lambda' = \Lambda - 4BT_c(\chi h)^2$ in the external magnetic field.

Finally, we note that at $t' = -3\Lambda'/2$ (which can be correct only in the magnetic field) the $2Q$ structure continuously transforms into the $2S$ one.

B. Phase transitions

In the absence of the external field, the sequence of phase transitions is somewhat trivial in comparison with the one described in Sec. III B. At $t \leq 3\Lambda/2$, $1S$ has lower free energy than $2S$. In the complementary domain $t > 3\Lambda/2$ the $1Q$ structure's free energy is always lower than f_{2Q} , which, in turn, is lower than f_{2S} . So upon temperature variation at $h = 0$ one has the $PM \leftrightarrow 1S \leftrightarrow 1Q$ sequence of continuous phase transitions at $t = 0$ and $t = 3\Lambda/2$, respectively.

In the external magnetic field, the following is an important observation: at $t_0 = 3\Lambda/2$ and h_0 , for which $BT_c(\chi h_0)^2 = \Lambda/4$, order parameters of all relevant phases are zero (see the previous section). The phases PM (equivalently, field-polarized phase), $1S$, $2S$, $1Q$, and $2Q$ are in perfect equilibrium at this *polycritical* point; slightly varying t and h , one can *continuously* get into each phase.

Now we can derive the phase boundaries at small t . First, there is a boundary between PM and $1S$ at

$$t_c^{(1)}(h) = 6BT_c \chi^2 h^2, \quad h \leq h_0. \quad (61)$$

At larger fields $h > h_0$ the $1S$ phase does not exist, and the PM phase has the boundary with the $2S$ one:

$$t_c^{(2)}(h) = \Lambda + 2BT_c \chi^2 h^2, \quad h > h_0. \quad (62)$$

Next, fixing $h < h_0$ and increasing t , one will have a continuous phase transition from $1S$ to $1Q$. It is governed by the equation $t' = 3\Lambda'/2$, which for these phases is invariant as a function of h and yields the vertical line

$$t_{1Q}(h) = \frac{3\Lambda}{2}, \quad h \leq h_0. \quad (63)$$

For $t > t_0$ there is a first-order transition from $1Q$ to $2Q$ at $t' = -3(1 + \sqrt{2})\Lambda'/2 \approx -3.6\Lambda'$ upon h increasing, or,

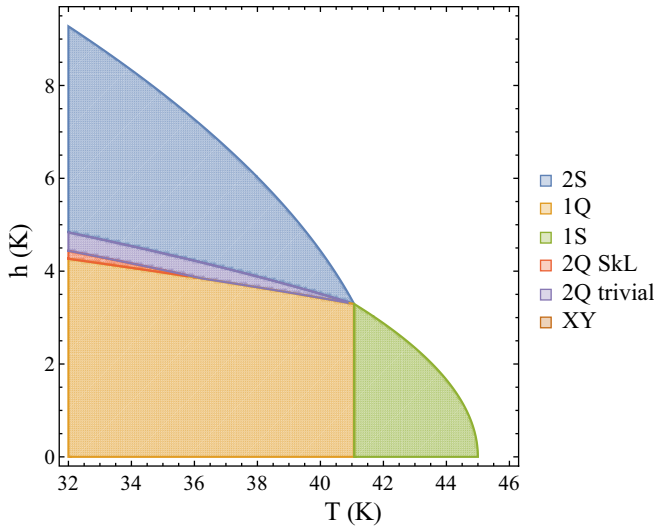


FIG. 5. Analytically obtained phase diagram for parameter set (69). In comparison with Fig. 3, the easy axes for both modulation vectors are along \mathbf{c} due to the single-ion anisotropy, which leads to crucial differences. In this case the square SkL (red region) emerges only at finite external magnetic field and not very close to the ordering temperature T_c . The conical XY phase appears at $T \lesssim 30$ K, where the mean-field approach is inapplicable. This phase diagram captures important features of the experimentally observed one for GdRu_2Si_2 [17].

equivalently,

$$t_S(h) = -3.6\Lambda + 20.4BT_c\chi^2h^2, \quad h > h_0. \quad (64)$$

Then, when $t' = -3\Lambda'/2$ there is a second-order transition between the $2Q$ and $2S$ phases, which yields

$$t_{2Q}(h) = -3\Lambda/2 + 12BT_c\chi^2h^2, \quad h > h_0. \quad (65)$$

The XY phase can emerge in the magnetic field via the spiral plane flop transition from the $1Q$ one. It can be shown that the corresponding field is [see Eq. (38)]

$$h_{SF} = \sqrt{\frac{\Lambda''}{4BT_c\chi^2}} > h_0. \quad (66)$$

As in Sec. III one can estimate the triple-point temperature; the counterpart of Eq. (44) reads

$$t_{tr} \approx 5.1\Lambda'' - 3.6\Lambda, \quad (67)$$

which also typically lies out of the theory applicability range (see the discussion in Sec. III C).

For nontrivial lattice topology in the $2Q$ phase (see Sec. IV), the condition $4s_1^2 > m^2 = \chi^2h^2$ should hold. We arrive at the same result [Eq. (47)] as in Sec. IV using Eq. (59), but with different $t_{2Q}(h)$ given by Eq. (65). Importantly, in the present case the condition

$$t_{SkL}(h) = t_{2Q}(h) + 9BT_c\chi^2h^2/4 < t_S(h) \quad (68)$$

provides an additional restriction of the topologically nontrivial part of the phase diagram, which approximately reads

$BT_c\chi^2h^2 > \Lambda/2.9$. So the square SkL part of the phase diagram starts at a certain $t > t_0$ (see Fig 5).

C. Qualitative description of the GdRu_2Si_2 phase diagram

Here we utilize the parameters of the exchange interaction and the dipolar tensor from (14). However, we add single-ion easy-axis anisotropy with $Z = 0.15$ K. This yields (all values are in kelvins).

$$\begin{aligned} \lambda_1 &\approx 4.3, & \lambda_0 &\approx 2.3, \\ \lambda_1 - \lambda_2 &\approx 0.25, & \lambda_1 - \lambda_3 &\approx 0.45, \end{aligned} \quad (69)$$

where the easy axis is the \mathbf{c} one due to the additional anisotropy.

The phase diagram obtained is shown in Fig. 5. First, we note that in this case the XY phase emerges only at $T \lesssim 30$ K, where our approach is inapplicable. Next, the topologically nontrivial square skyrmion lattice is a narrow red wedge in Fig. 5 (but starting at temperatures for which the developed approach should work at least qualitatively). This should be contrasted with the large SkL domain for in-plane easy axes (see Fig. 3). Finally, we point out that the phase diagram (Fig. 5) has important similarities with the one in Ref. [17]. For instance, its topologically nontrivial narrow part starts at finite magnetic field and at a certain temperature not very close to T_c . Thus, we suggest that additional experiments determining the phase boundaries in GdRu_2Si_2 are in order.

VI. DISCUSSION AND CONCLUSION

To conclude, we showed that magnetic dipolar interaction can stabilize a square skyrmion lattice in centrosymmetric tetragonal frustrated antiferromagnets. The size of the corresponding magnetic unit cell is of the order of several nanometers.

We found that the hierarchy of the axes is crucial for the magnetic-field-temperature phase diagram and provided an analytical mean-field consideration of the two possible cases in the high-temperature domain. If the easy axes for both modulation vectors are collinear, the phase diagram resembles the recently observed one for GdRu_2Si_2 [17]. However, there are important analytical predictions which can be checked experimentally: the square SkL region is only part of the double- Q elliptical phase, which at larger fields continuously transforms into the double- Q vortical structure. Near the latter phase transition the spin component along the external field is always positive, and the structure is topologically trivial.

Importantly, the conical phase emerges in a certain part of the phase diagram in our analysis. However, using parameters relevant to GdRu_2Si_2 , we show that our approach fails in that region. Nevertheless, in general, the conical phase can be pronounced in the phase diagram. So further studies devoted to low-temperatures are important. For example, in Ref. [27] it was shown that, depending on the parameters, the conical phase can or cannot appear in frustrated antiferromagnets with only single- Q modulated structures possible. Moreover, at low temperatures skyrmion textures contain lots of non-negligible additional harmonics. The construction of the corresponding lattice and its energy calculation, usually a hard problem itself [37], in the present model with dipolar forces becomes

very challenging even numerically due to their long-range character. Finally, we note that the symmetry-allowed compass anisotropy terms can be easily included in the present theory, which could be important in the experimental data description.

ACKNOWLEDGMENTS

I am grateful to V. A. Ukleev and A. V. Syromyatnikov for valuable discussions. The reported study was supported by the Foundation for the Advancement of Theoretical Physics and Mathematics “BASIS.”

-
- [1] T. Skyrme, *Nucl. Phys.* **31**, 556 (1962).
 [2] A. Belavin and A. Polyakov, *JETP Lett.* **22**, 245 (1975).
 [3] A. N. Bogdanov and D. Yablonskii, *Zh. Eksp. Teor. Fiz.* **95**, 178 (1989) [*Sov. Phys. JETP* **68**, 100 (1989)].
 [4] A. Bogdanov and A. Hubert, *J. Magn. Magn. Mater.* **138**, 255 (1994).
 [5] I. Dzyaloshinsky, *J. Phys. Chem. Solids* **4**, 241 (1958).
 [6] T. Moriya, *Phys. Rev.* **120**, 91 (1960).
 [7] S. Mühlbauer, B. Binz, F. Jonietz, C. Pfleiderer, A. Rosch, A. Neubauer, R. Georgii, and P. Böni, *Science* **323**, 915 (2009).
 [8] A. Fert, N. Reyren, and V. Cros, *Nat. Rev. Mater.* **2**, 1 (2017).
 [9] A. N. Bogdanov and C. Panagopoulos, *Nat. Rev. Phys.* **2**, 492 (2020).
 [10] A. Fert, V. Cros, and J. Sampaio, *Nat. Nanotechnol.* **8**, 152 (2013).
 [11] A. Neubauer, C. Pfleiderer, B. Binz, A. Rosch, R. Ritz, P. G. Niklowitz, and P. Böni, *Phys. Rev. Lett.* **102**, 186602 (2009).
 [12] B. Göbel, I. Mertig, and O. A. Tretiakov, *Phys. Rep.* **895**, 1 (2021).
 [13] A. Leonov and M. Mostovoy, *Nat. Commun.* **6**, 8275 (2015).
 [14] T. Kurumaji, T. Nakajima, M. Hirschberger, A. Kikkawa, Y. Yamasaki, H. Sagayama, H. Nakao, Y. Taguchi, T.-h. Arima, and Y. Tokura, *Science* **365**, 914 (2019).
 [15] Y. Tokura, S. Seki, and N. Nagaosa, *Rep. Prog. Phys.* **77**, 076501 (2014), and references therein.
 [16] T. Kurumaji, *Phys. Sci. Rev.* **5**, 20190016 (2019), and references therein.
 [17] N. D. Khanh, T. Nakajima, X. Yu, S. Gao, K. Shibata, M. Hirschberger, Y. Yamasaki, H. Sagayama, H. Nakao, L. Peng, K. Nakajima, R. Takagi, T.-H. Arima, Y. Tokura, and S. Seki, *Nat. Nanotechnol.* **15**, 444 (2020).
 [18] S. Hayami and Y. Motome, *Phys. Rev. B* **103**, 024439 (2021).
 [19] Z. Wang, Y. Su, S.-Z. Lin, and C. D. Batista, *arXiv:2011.04033*.
 [20] A. Hubert and R. Schäfer, *Magnetic Domains: The Analysis of Magnetic Microstructures* (Springer-Verlag, Berlin, Heidelberg, 1998).
 [21] H. Shiba, *Solid State Commun.* **41**, 511 (1982).
 [22] R. S. Gekht, *Sov. Phys. Usp.* **32**, 871 (1989), and references therein.
 [23] T. Sato, H. Kadowaki, H. Masudo, and K. Iio, *J. Phys. Soc. Jpn.* **63**, 4583 (1994).
 [24] O. I. Utesov and A. V. Syromyatnikov, *Phys. Rev. B* **95**, 214420 (2017).
 [25] R. White, *Quantum Theory of Magnetism*, Springer Series in Solid-State Sciences (Springer-Verlag, Berlin, Heidelberg, 1983).
 [26] O. I. Utesov and A. V. Syromyatnikov, *Phys. Rev. B* **100**, 054439 (2019).
 [27] O. I. Utesov and A. V. Syromyatnikov, *J. Magnetism and Magnetic Mater.* **527**, 167732 (2021).
 [28] M. Ślaski, A. Szytuła, J. Leciejewicz, and A. Zygunt, *J. Magn. Magn. Mater.* **46**, 114 (1984).
 [29] S. Banerjee, O. Erten, and M. Randeria, *Nat. Phys.* **9**, 626 (2013).
 [30] J. Chen, D.-W. Zhang, and J.-M. Liu, *Sci. Rep.* **6**, 29126 (2016).
 [31] M. H. Cohen and F. Keffer, *Phys. Rev.* **99**, 1128 (1955), and references therein.
 [32] R. Gekht, *Zh. Eksp. Teor. Fiz.* **87**, 2095 (1984) [*Sov. Phys. JETP* **60**, 1210 (1984)].
 [33] In energy units $h_{\text{sat}} \approx S(J_{\mathbf{k}_x} - J_0)$ if one neglects small anisotropy and shape-dependent corrections; see, e.g., Ref. [27].
 [34] A. I. Akhiezer, S. Peletminskii, and V. G. Baryakhtar, *Spin Waves* (North-Holland, Amsterdam, Netherlands, 1968).
 [35] O. I. Utesov and A. V. Syromyatnikov, *Phys. Rev. B* **98**, 184406 (2018).
 [36] X. Yu, W. Koshibae, Y. Tokunaga, K. Shibata, Y. Taguchi, N. Nagaosa, and Y. Tokura, *Nature (London)* **564**, 95 (2018).
 [37] V. E. Timofeev, A. O. Sorokin, and D. N. Aristov, *JETP Lett.* **109**, 207 (2019).